

Generating soliton trains through Floquet engineering

P. Blanco-Mas and C.E. Creffield

Departamento de Física de Materiales, Universidad Complutense de Madrid, E-28040 Madrid, Spain

(Dated: April 13, 2023)

We study a gas of interacting ultracold bosons held in a parabolic trap in the presence of an optical lattice potential. Treating the system as a discretised Gross-Pitaevskii model, we show how Floquet engineering, by rapidly “shaking” the lattice, allows the ground-state of the system to be converted into a train of bright solitons by inverting the sign of the hopping energy. We study how the number of solitons produced depends on the system’s nonlinearity and the curvature of the trap, show how the technique can be applied both in the high and low driving-frequency regimes, and demonstrate the phenomenon’s stability against noise. We conclude that the Floquet approach is a useful and stable method of preparing solitons in cold atom systems.

I. INTRODUCTION

A soliton is a localized excitation in a medium that preserves its shape in time as it travels. First observed in water waves propagating in narrow channels [1], they are ubiquitous in Nature, arising in such diverse contexts as laser pulses in optical fibers [2], the dynamics of tsunamis [3], and kinks moving along DNA [4]. Their stability arises from a balance between a localized wavepacket’s intrinsic tendency to spread in time, and a non-linear attractive interaction which opposes this spreading.

Bose-Einstein condensates (BECs) are particularly interesting candidates to study soliton formation, as the systems are very clean and highly controllable, and, in particular, the interatomic interaction can be manipulated accurately in the laboratory. When the interaction is repulsive the BEC is stable. However, if the interaction is rapidly changed to be attractive the BEC is rendered vulnerable to modulational instability, causing it to break up into ripples which are then focused by the interaction to form solitons. In this way, soliton trains have been produced in BECs of lithium-7 atoms [5, 6], rubidium-85 [7] and in cesium-133 [8, 9], using the Feshbach resonance technique to rapidly change the interaction strength. More recently, an alternative method of controlling the atomic interaction has been developed which involves coupling internal atomic states with different scattering lengths with an RF field, which has been successfully used [10] to produce solitons in BECs of potassium-39.

In this work we revisit a protocol proposed by Carr and Brand (CB) [11, 12] for converting a trapped BEC into a soliton train. It consists of two parts. Initially a BEC with a repulsive interaction is held in a trapping potential, as normal. This stable situation is then perturbed by flipping the sign of the interatomic interaction, while simultaneously inverting the trap so that it becomes expulsive. If we write the Hamiltonian of the system as a sum of the kinetic energy T , the trapping potential V , and the interaction term U , we can schematically represent this process as

$$H = T + V + U \implies T - V - U . \quad (1)$$

This protocol thus requires control over both the inter-

action strength and the sign of the trap, which may not always be experimentally feasible. We instead propose to use a variant of this technique by addressing a *single* parameter: the sign of the kinetic energy. This process can be represented instead as

$$H = T + V + U \implies -T + V + U , \quad (2)$$

which is clearly equivalent to the CB protocol, but with an overall minus sign.

The required inversion of the kinetic energy, equivalent to endowing the atoms with a negative effective mass, can be achieved by a technique known as “Floquet engineering” [13] by applying an external driving field which oscillates periodically in time. The dynamics of the system can then be factored into a rapid micromotion oscillating at the same frequency as the driving field, and an effective static Hamiltonian H_{eff} . The parameters of H_{eff} can be controlled very precisely by the driving field, and in particular “shaking” a tight-binding lattice model by rapidly oscillating the lattice in space, allows the intersite tunneling to be coherently manipulated. The intersite tunneling, for example, can be tuned to zero to produce the effect known as “coherent destruction of tunneling” (CDT) [14], it can be rendered complex to allow the system to simulate the effect of a synthetic magnetic field [15–17], or its sign can be inverted [18, 19], to provide a negative effective mass.

Inverting the sign of the effective mass has been previously used in a static system to produce gap solitons [20], by moving a trapped condensate to the edge of the first Brillouin zone (FBZ) where the dispersion relation has negative curvature. More recently, Ref. [21] performed an experiment using Floquet engineering to flip the sign of the tunneling by high-frequency shaking of a cesium BEC to obtain a solitonic wavepacket at the center of the FBZ. By employing a similar driving of this type we will show how Floquet engineering can be used in conjunction with varying the trapping potential and the magnitude of the atomic interaction to create stable soliton trains containing a specific number of solitons. We will then go on to examine both the high and low frequency driving regimes, and show that soliton formation occurs in both. Having the ability to vary the driving frequency in this way gives the flexibility to avoid exciting the atoms to

a higher band at high driving frequencies, and also to evade parametric resonances [22], which would otherwise heat and eventually destroy the condensate. Finally we will study the effect of the phase of the driving on the protocol, and demonstrate the scheme's remarkably high robustness to noise.

II. METHOD

A. Model

A BEC held in a trap potential can be described well by the Gross-Pitaevskii Hamiltonian

$$H_{GP} = \frac{-\hbar^2}{2m} \partial_x^2 + V(x) + g |\psi(x)|^2, \quad (3)$$

where g is the interatomic coupling constant, proportional to the s -wave scattering length, m is the atomic mass, and the condensate wavefunction, $\psi(x)$, is normalized to one. The trapping potential is denoted by $V(x)$, and will be taken to be quadratic, $V(x) = V_0 x^2$, where the distance x is measured from the center of the system. If we now discretise space by imposing an optical lattice potential, Eq. 3 can be rewritten in second-quantized form,

$$H_{\text{latt}} = -J \sum_j (a_j a_{j+1}^\dagger + \text{H.c.}) + \sum_j V(x_j) n_j + g \sum_j n_j^2, \quad (4)$$

where the kinetic energy is now given in terms of the tunneling J between nearest-neighbor lattice sites, a_j/a_j^\dagger are the annihilation / creation operators for a boson on site j , and $n_j = a_j^\dagger a_j$ is the standard number operator. Henceforth we will take $\hbar = 1$, and measure all energies and frequencies in units of J , and write all distances in units of the lattice constant.

We will take the initial state for the simulations to be the ground state of Hamiltonian (4). This is obtained by starting with the solution for $g = 0$ (a Gaussian) and evolving it under Eq. 4 in imaginary time, maintaining the correct normalization, until convergence is achieved. The results for several different values of g are shown in Fig. 1, and the evolution from a narrow Gaussian distribution to the broader inverted parabolic form predicted by the Thomas-Fermi approximation in the limit of large g is clearly visible.

We now wish to introduce the time-dependent driving potential. If the optical lattice is periodically oscillated in space, or “shaken”, an observer in the rest frame of the lattice perceives an inertial force described by a time-dependent lattice tilt, resulting in the Hamiltonian

$$H(t) = H_{\text{latt}} + K(t) \sum_j j n_j, \quad (5)$$

where $K(t)$ describes the form of the shaking. For the common case of sinusoidal shaking, this function can be

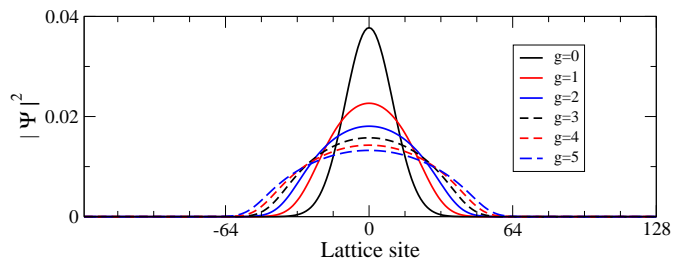


FIG. 1. Probability density of the ground state of the lattice GPE (Eq. 4) for different values of the non-linearity g . The curvature of the trap is given by $V_0 = 2 \times 10^{-5}$. Note how the wavefunction evolves from a Gaussian for $g = 0$, to a broader, more flattened form as g increases and the system approaches the Thomas-Fermi limit.

written as $K(t) = K \cos(\omega t + \phi)$, where ω is the frequency of the driving, K is its amplitude, and for generality we have included a driving-phase ϕ . All numerical results were obtained by first preparing the initial state using the imaginary time relaxation method described above, and then integrating this state in time under Eq. 5, using a fourth-order Runge-Kutta routine.

B. Floquet engineering

As the time-dependent driving (5) is T -periodic, $H(t) = H(t + nT)$, solutions of the time-dependent Schrödinger equation are of Floquet form

$$[i\partial_t - H(t)] \psi_n(t) = \epsilon_n \psi_n(t) \quad (6)$$

where the Floquet states $\psi_n(t)$ have the same T -periodicity as the Hamiltonian, and provide a complete basis to describe the time evolution of the driven system. The eigenvalues ϵ_n are called the quasienergies, and govern the long-term dynamics of the system, as the time-dependence of the Floquet states only operates over timescales within each driving period, providing the so-called “micromotion” [13] of the system.

The quasienergies can be obtained as the eigenenergies of an effective static Hamiltonian, H_{eff} , which depends on the parameters and form of the driving. The process of Floquet engineering then consists of choosing the appropriate driving function to produce the desired form of H_{eff} , and thus the quasienergies. In general it is difficult to obtain closed-form solutions for the quasienergies for a given drive. It is possible, however, to obtain expressions for H_{eff} as series expansions in inverse frequency, such as the Magnus series [23] and the Van Vleck series [24], which become exact in the limit of infinite driving frequency. To first order, it can be shown that for a sinusoidally-driven two-level system the quasienergies are given by [25] $\epsilon_{\pm} = \pm J \mathcal{J}_0(K/\omega)$, where \mathcal{J}_0 is the zeroth Bessel function of the first kind. Fig. 2 shows the

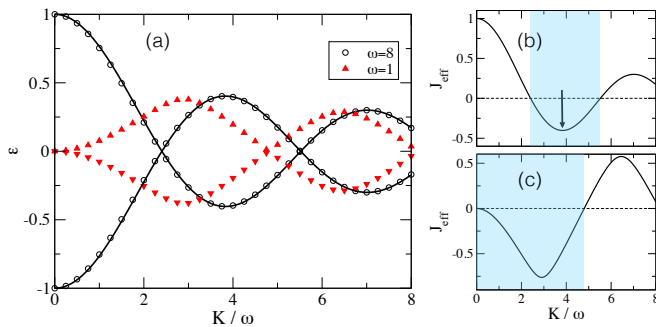


FIG. 2. (a) Quasienergies for the two-level model. Black solid lines show the first-order approximation $\epsilon = \pm \mathcal{J}_0(K/\omega)$ which becomes exact in the limit $\omega \rightarrow \infty$. Black circles show the exact numerical results for $\omega = 16$; at this high-frequency the results are excellently approximated by the perturbative result. The red triangles show the quasienergies for $\omega = 1$, which differ considerably from the Bessel function behaviour of the high frequency results. b) J_{eff} for $\omega = 16$; note how this vanishes at $K/\omega = 2.404$, and is negative in the shaded region between the first and second zeros of \mathcal{J}_0 . The arrow marks $K/\omega = 3.80$, the value used in the Floquet engineering method. c) J_{eff} for $\omega = 1$. Again, the shaded region indicates where the effective tunneling is negative. The quantities ϵ and J_{eff} are measured in units of J (see text).

excellent agreement between this result and the numerical results for a two-level system driven at $\omega = 16$. Good agreement continues to be obtained as long as $\omega > J$: the high-frequency regime. However, for lower frequencies the quasienergies behave differently, as can be seen for the case of $\omega = 1$, indicating that more terms [26] must be included in the series.

The effective tunneling between the levels is proportional to the difference between the quasienergies, $J_{\text{eff}} = (\epsilon_+ - \epsilon_-)/2$, and thus in the high-frequency limit the effective tunneling is given by

$$J_{\text{eff}} = J \mathcal{J}_0(K/\omega) . \quad (7)$$

Altering the parameter K/ω therefore allows J_{eff} to be tuned to a desired value. In particular, if we set $K/\omega = 2.404$ (the first zero of the Bessel function) the two quasienergies become degenerate, as can be seen in Fig. 2a, and the effective tunneling vanishes, producing CDT. Increasing K/ω beyond this value causes J_{eff} to become negative in the interval between the first and second zeros of \mathcal{J}_0 (the shaded region in Fig. 2 b), which is thus the region of interest for our soliton generation method (2).

Proceeding to an N -site lattice system, the quasienergies now present a band-like structure [27]

$$\epsilon_n = -2J_{\text{eff}} \cos k_n , \quad (8)$$

where k_n are the permitted momenta in the FBZ, and J_{eff} is the same intersite tunneling discussed above (Eq. 7). Accordingly we can regulate the effective mass of

a particle moving in the lattice in the same way that we can control the tunneling in the two-level model, by appropriately choosing the value of K/ω .

III. RESULTS

Soliton generation – In Fig. 3 we show the results of applying the Floquet protocol to a system with non-linearity parameter $g = 2$. The system was prepared in its ground state, and then at $t = 0$ the driving potential was suddenly turned on, with phase $\phi = 0$, and a frequency of $\omega = 16$ placing the system firmly in the high-frequency regime. As shown in Fig. 2b, the amplitude of the driving was chosen to be $K/\omega = 3.80$ that is, the first minimum of Eq. 7, the corresponding value of $J_{\text{eff}} = -0.403$ being the largest negative value possible for the effective tunneling.

When the driving potential is applied, small ripples develop in the profile of the condensate. As Carr and Brand demonstrated, the dominant source of these ripples is self-interference of the condensate wavefunction, which causes them to develop first at the edges of the wavepacket. Modulational instability causes the ripples to grow in amplitude, and they are then focused by the nonlinearity into forming sharp peaks with a typical soliton profile. For this value of the nonlinearity the initial wavepacket divides into three solitons. The one which forms near the center of the trap remains essentially stationary over the remainder of the time evolution, while the other two accelerate away at an exponentially increasing velocity. Although the trapping potential does not change during the protocol, the solitons have a negative effective mass due to the inversion of J_{eff} , and so “fall uphill” against the potential and are accelerated outwards, just like a normal particle in an inverted potential. Note that once formed, the solitons are stable, and retain their form throughout their trajectory.

Raising the value of g reveals that the number of solitons produced in a trap with a given curvature increases weakly as a function of the nonlinearity, as observed previously in Refs. [28, 29]. The trap curvature can also be used as a parameter to control the soliton number. We show the combined effect of these factors in Fig. 4a. From this plot it is clear that high soliton numbers are favored by a high value of the nonlinearity and a low trap curvature. This can be understood qualitatively by a simple scaling argument. The growth of the ripples is governed by the most unstable Bogoliubov mode, the wavelength of which [28] is related to the healing length of the condensate, ξ . The other length scale of the problem is the harmonic oscillator length ℓ which gives an estimate for the effective width of the initial wavepacket. On dimensional grounds, the number of solitons will vary approximately as the ratio of these lengths

$$n \sim \xi/\ell \sim \left(g/\sqrt{V_0}\right)^{1/2} , \quad (9)$$

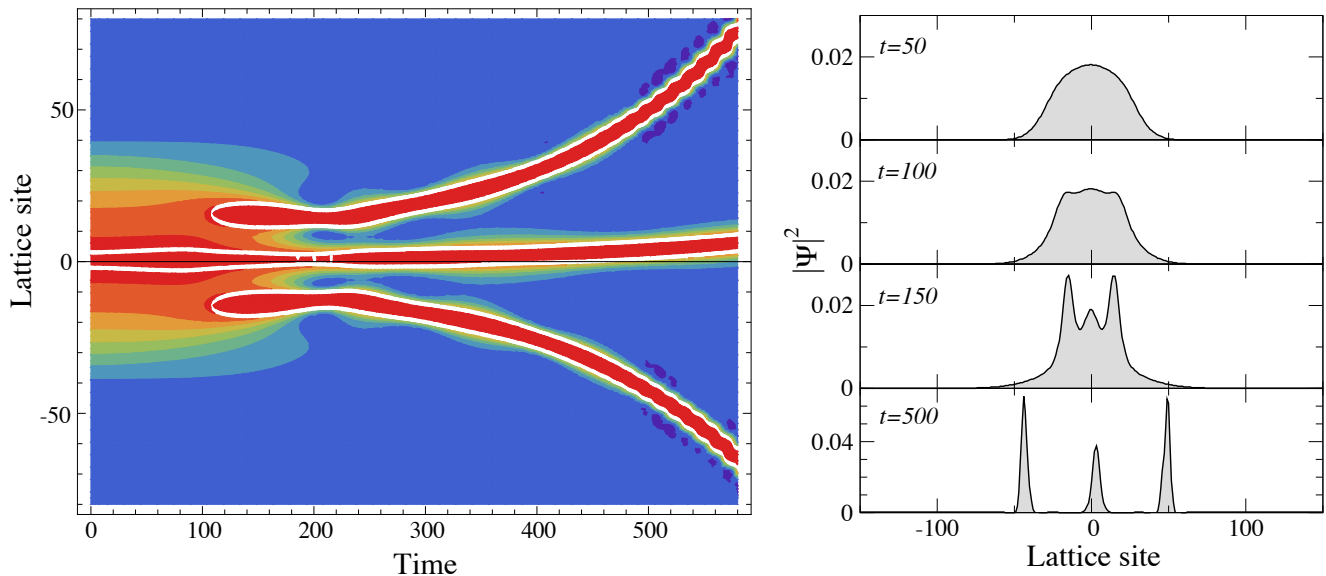


FIG. 3. Soliton generation using the Floquet engineering protocol (2). Physical parameters: 512 lattices sites, $V_0 = 2 \times 10^{-5}$, $g = 2$, and the driving frequency $\omega = 16$. Left: contour plot of the condensate density $|\psi(x, t)|^2$. The system is initialized in its ground state, and at $t = 0$ the driving potential is applied. At $t = 100$ ripples begin to form in the condensate, which gradually focus into three solitons. The central soliton remains close to the center of the lattice, remaining in unstable equilibrium with the lattice potential, while the other two solitons accelerate exponentially away. Right: cross sections through the condensate at different times. The ripples form initially at the edges of the wavepacket, indicating they arise from self-interference, and then sharpen into the typical soliton shape.

in agreement with the trends observed.

To examine this behaviour more quantitatively, we plot in Fig. 4b the critical value of the nonlinearity parameter, g_c , at which the number of solitons produced in the system changes from two to three – that is, the lowest boundary curve plotted in Fig. 4a. According to Eq. 9, this quantity should vary as $g_c \sim \sqrt{V_0}$. As can be seen, the data can indeed be fitted with reasonable accuracy by this expression.

Low-frequency regime – The results presented so far have been for $\omega = 16$, which is well within the high-frequency regime. The results obtained are essentially identical to those obtained by performing the simulations without the time-dependent driving, but setting the value of J to $J_{\text{eff}} = -0.403$ by hand at $t = 0$, which we shall term the “switched protocol”. The excellent agreement between the results indicates how well the Floquet protocol duplicates the switched protocol for this frequency.

As ω is lowered we should expect this agreement to reduce, as more terms must be included in the Magnus expansion, and H_{eff} can no longer be approximated as a nearest-neighbor hopping Hamiltonian with a single effective tunneling. Perhaps surprisingly, although the amplitude and position of the generated solitons alter slightly for smaller values of ω , the process of soliton formation itself remains robust. The important point is just that the nearest-neighbor tunneling must become negative. Although the positions of quasienergy degeneracies

will drift away from the zeros of the Bessel function as the frequency is reduced [25], there will nonetheless still be some intervals over which J_{eff} will be negative.

As an example, in Fig. 2c, we plot the effective tunneling for a system at a low driving frequency of $\omega = 1$. As we noted previously, J_{eff} is related to the difference of the quasienergies, but unlike the high-frequency case, in this instance we do not know which quasienergy corresponds to ϵ_+ and which to ϵ_- . As a result, even knowing the values of the quasienergies we are uncertain of the sign of J_{eff} . Simulating the driven system in a lattice with an additional static tilt reveals that an initial wavepacket moves up the potential for $K/\omega < 4.8$, indicating that its effective mass is negative, while it moves down the potential for higher driving amplitudes, corresponding to its effective mass being positive. Accordingly, driving the system at $K/\omega = 3.8$, as done in the high-frequency case, should also produce solitons.

We show the results in Fig. 5 for three different driving frequencies. At the sample time used, $t = 300$, the switched protocol produces in three solitons. For a driving frequency of $\omega = 16$, the result is essentially indistinguishable for the switched protocol. Lowering the driving frequency to $\omega = 4$ again gives a very similar result: although the three solitons produced have slightly different positions and amplitudes, the differences from the $\omega = 16$ result are very minor. Taking now the value $\omega = 1$, well outside the high-frequency regime, again gives a very sim-

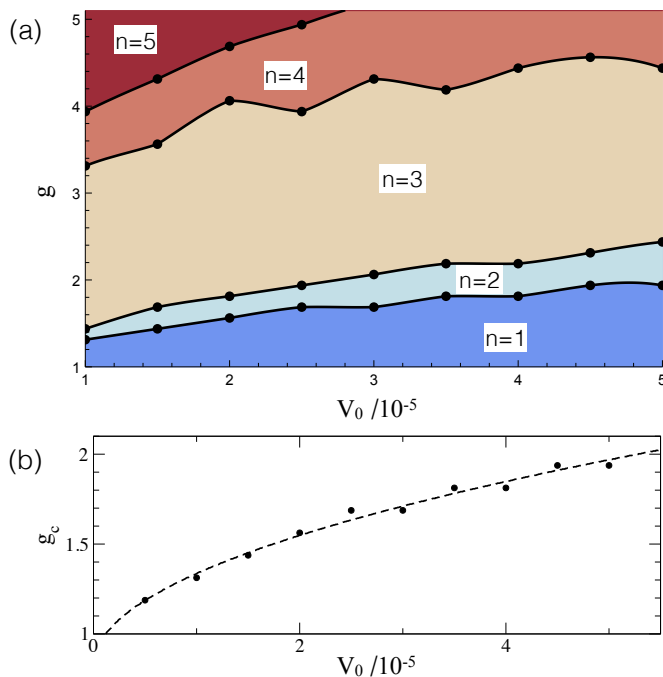


FIG. 4. a) Number of solitons produced as the trap curvature V_0 and the nonlinearity g , both measured in units of J , are varied. The number of solitons increases for high g and low V_0 , as predicted by Eq. 9. In all cases a lattice of 256 sites was used. b) Plot of the critical interaction strength, g_c , at which the system changes from producing two solitons to producing three. The dashed line is a least squares fit to $g_c = a_1 + a_2\sqrt{V_0}$, where a_1 and a_2 are fitting parameters, which describes the behaviour with reasonable accuracy.

ilar result. Using a high driving frequency is thus not a necessary requirement for this technique, as long as J_{eff} changes sign.

Effect of phase – The amplitude of the driving is set through the requirement $K/\omega = 3.8$, and we have shown that the effect is robust to varying the driving frequency, ω . This leaves one last parameter in the driving to consider: the phase, ϕ . We have so far used cosinusoidal driving, that is, $\phi = 0$. If we instead use sinusoidal driving ($\phi = \pi/2$) we see no sign of any soliton creation. The wavepacket instead sloshes from side to side of the trapping potential. This effect is produced by the so-called kick-operator [13]. As shown in Ref. [30], when ϕ is not zero, the driving imprints a phase onto the condensate which excites it into motion. For the type of driving we consider the full expression for the effective tunneling is given in the high-frequency limit by

$$J_{\text{eff}} = J e^{-i[K/\omega] \sin \phi} \mathcal{J}_0(K/\omega), \quad (10)$$

which clearly reduces to Eq. 7 for $\phi = 0$. While the same Bessel function renormalization of the modulus of the tunneling still happens for sinusoidal driving, the additional phase factors mean that J_{eff} does not flip sign

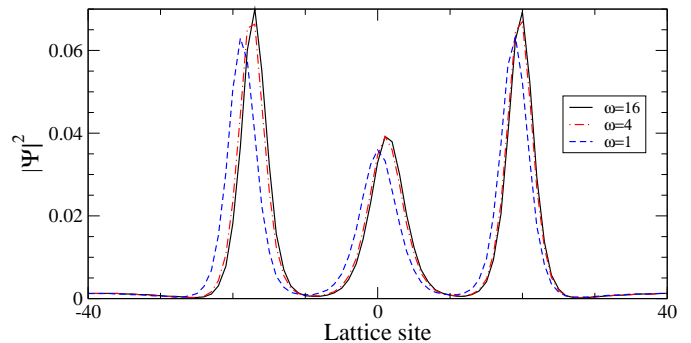


FIG. 5. Soliton development at $t = 300$ for three different driving frequencies. In the high frequency regime, $\omega = 16$ (solid black line), the results obtained are indistinguishable from the switched protocol. For $\omega = 4$ (dash-dotted red line) the solitons produced strongly resemble the high frequency result, although small differences are visible. At low frequency, $\omega = 1$ (dashed blue line), the differences are larger, but qualitatively a very similar result is still obtained. System parameters: 512 lattice sites, $V_0 = 0.00002$ and $g = 2$.

when $K/\omega = 3.80$. The driving instead delivers a kick to the condensate, giving it an initial velocity $v_0 = K/\omega$, and thus causing it to make harmonic oscillations about the center of the trap.

Noise – We finally consider how stable the soliton creation process is to noise on the initial state, since in experiment it is clearly impossible to prepare the desired initial state with complete fidelity. We have so far used the ground state, $\psi^0(x)$, as the initial state, and we will now add random noise to it

$$\psi(x, t = 0) = \psi^0(x) + r(x)\gamma, \quad (11)$$

where r is a random variable uniformly distributed over $(-1, 1)$, and γ sets the amplitude of the noise. After the noise has been added to both the real and imaginary components of $\psi^0(x)$, the resulting state is normalized to unity as usual, and used as the initial state of the simulation.

We show the results for two different noise levels in Fig. 6. For the given system parameters, $V = 2 \times 10^{-5}$ and $g = 2$, we expect to produce three solitons, as seen previously in Fig. 3. For $\gamma = 0.01$ (Fig. 6a) the initial state already appears notably irregular, but the process indeed gives rise to three well defined solitons. Unlike in the clean system, the seeds for soliton formation are now dominated by the imposed random fluctuations in the condensate wavefunction, rather than by self-interference of the condensate. As a result the positions of the solitons are randomly shifted in position with respect to the clean system, and the solitons are more equal in size, as they began forming at essentially the same time. Further increasing the noise level to $\gamma = 0.05$ produces two solitons instead of the three expected. Nonetheless it is striking that even in the presence of such a high level of noise, the

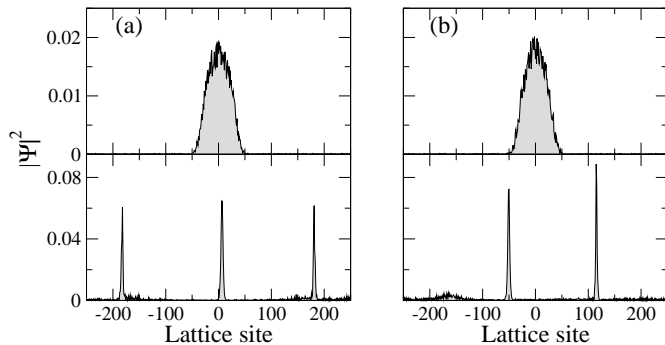


FIG. 6. Effect of noise on soliton generation. (a) Above: initial state with $\gamma = 0.01$. Below: the particle density of the system at $t = 300$. Just as in the clean system (Fig. 3), three solitons form. (b) Above: initial state with $\gamma = 0.05$. Below: at $t = 300$ the system has evolved to present just two solitons, the random noise having affected details of the soliton generation process. Physical parameters: 512 lattice sites, $V = 2 \times 10^{-5}$, $g = 2$.

process still produces clearly identifiable solitons that are easily detectable above the background noise level

IV. CONCLUSIONS

In summary, we have shown how Floquet engineering may be used to implement a protocol based on the CB method for converting a trapped condensate into a train of solitons. It has the advantage that only one control parameter needs to be altered, and as it does not involve controlling the interparticle interaction, it is applicable to atomic species for which this control is not easily available, such as those like rubidium-87 which lack a convenient Feshbach resonance. The method consists

of using Floquet physics to invert the sign of the inter-site tunneling, or equivalently, to give the condensate atoms a negative effective mass. Modulational instability then causes the initial state to break up into a train of spatially-localized pulses, which then self-focus into solitons under the influence of the nonlinear interaction. We have demonstrated how the curvature of the trap and the magnitude of the atomic interaction can be used to deterministically prepare trains of a given number of solitons. Unlike many applications of Floquet engineering, the method is not restricted to the high-frequency regime, but works equally well for lower driving frequencies, which have the advantage of avoiding driving the atoms into higher bands. In experiment, soliton generation in the low-frequency regime may be harder to attain due to the increased rate of heating [22] destroying the coherence of the condensate. Nonetheless, experiments [18] have reported coherent control of the tunneling down to frequencies of $\omega = 0.3J$, well into the low frequency regime, and once formed the solitons are able to self-cool [11] by emitting small bursts of atoms. Finally we would like to emphasise the remarkable stability of the method with respect to noise. The modulational instability is seeded by the most unstable Bogoliubov mode, and as this typically has a fairly long wavelength, noise on shorter length scales has relatively little effect. The repeatability and excellent control afforded by this method make it an excellent tool to investigate soliton dynamics and collisions, and hold out the prospect of using such soliton trains for precision measurement applications such as atom interferometry.

ACKNOWLEDGMENTS

This work was supported by the Universidad Complutense de Madrid through grant no. FEI-EU-19-12.

-
- [1] J. S. Russell, *Report of the British Association for the Advancement of Science*, 311 (1844).
 - [2] A. Hasegawa, *Opt. Photon. News* **13**, 33 (2002).
 - [3] A. Constantin and D. Henry, *Zeitschrift für Naturforschung A* **64**, 65 (2009).
 - [4] A. Davydov, *Journal of Theoretical Biology* **38**, 559 (1973).
 - [5] K. E. Strecker, G. B. Partridge, A. G. Truscott, and R. G. Hulet, *Nature* **417**, 150 (2002).
 - [6] L. Khaykovich, F. Schreck, G. Ferrari, T. Bourdel, J. Cubizolles, L. D. Carr, Y. Castin, and C. Salomon, *Science* **296**, 1290 (2002).
 - [7] S. L. Cornish, S. T. Thompson, and C. E. Wieman, *Phys. Rev. Lett.* **96**, 170401 (2006).
 - [8] T. Mežnaršič, T. Arh, J. Brence, J. Pišljarič, K. Gosar, Ž. Gosar, R. Žitko, E. Zupanič, and P. Jeglič, *Phys. Rev. A* **99**, 033625 (2019).
 - [9] A. Di Carli, C. D. Colquhoun, G. Henderson, S. Flannigan, G.-L. Oppo, A. J. Daley, S. Kuhr, and E. Haller, *Phys. Rev. Lett.* **123**, 123602 (2019).
 - [10] J. Sanz, A. Frölian, C. S. Chisholm, C. R. Cabrera, and L. Tarruell, *Phys. Rev. Lett.* **128**, 013201 (2022).
 - [11] L. D. Carr and J. Brand, *Phys. Rev. A* **70**, 033607 (2004).
 - [12] L. D. Carr and J. Brand, *Phys. Rev. Lett.* **92**, 040401 (2004).
 - [13] A. Eckardt, *Rev. Mod. Phys.* **89**, 011004 (2017).
 - [14] F. Grossmann, T. Dittrich, P. Jung, and P. Hänggi, *Phys. Rev. Lett.* **67**, 516 (1991).
 - [15] M. Aidelsburger, M. Atala, M. Lohse, J. T. Barreiro, B. Paredes, and I. Bloch, *Phys. Rev. Lett.* **111**, 185301 (2013).
 - [16] H. Miyake, G. A. Siviloglou, C. J. Kennedy, W. C. Burton, and W. Ketterle, *Phys. Rev. Lett.* **111**, 185302 (2013).

- [17] C. E. Creffield, G. Pieplow, F. Sols, and N. Goldman, *New Journal of Physics* **18**, 093013 (2016).
- [18] H. Lignier, C. Sias, D. Ciampini, Y. Singh, A. Zenesini, O. Morsch, and E. Arimondo, *Phys. Rev. Lett.* **99**, 220403 (2007).
- [19] A. Zenesini, H. Lignier, D. Ciampini, O. Morsch, and E. Arimondo, *Phys. Rev. Lett.* **102**, 100403 (2009).
- [20] B. Eiermann, T. Anker, M. Albiez, M. Taglieber, P. Treutlein, K.-P. Marzlin, and M. K. Oberthaler, *Phys. Rev. Lett.* **92**, 230401 (2004).
- [21] M. Mitchell, A. Di Carli, G. Sinuco-León, A. La Rooij, S. Kuhr, and E. Haller, *Phys. Rev. Lett.* **127**, 243603 (2021).
- [22] S. Lellouch, M. Bukov, E. Demler, and N. Goldman, *Phys. Rev. X* **7**, 021015 (2017).
- [23] S. Blanes, F. Casas, J. Oteo, and J. Ros, *Physics Reports* **470**, 151 (2009).
- [24] A. Eckardt and E. Anisimovas, *New Journal of Physics* **17**, 093039 (2015).
- [25] C. Creffield, *Phys. Rev. B* **67**, 165301 (2003).
- [26] J. C. A. Barata and W. F. Wreszinski, *Phys. Rev. Lett.* **84**, 2112 (2000).
- [27] C. E. Creffield, *Phys. Rev. A* **79**, 063612 (2009).
- [28] J. H. V. Nguyen, D. Luo, and R. G. Hulet, *Science* **356**, 422 (2017).
- [29] P. J. Everitt, M. A. Sooriyabandara, M. Guasoni, P. B. Wigley, C. H. Wei, G. D. McDonald, K. S. Hardman, P. Manju, J. D. Close, C. C. N. Kuhn, S. S. Szigeti, Y. S. Kivshar, and N. P. Robins, *Phys. Rev. A* **96**, 041601 (2017).
- [30] C. E. Creffield and F. Sols, *Phys. Rev. Lett.* **100**, 250402 (2008).